Comparison of Different Motor Design Drives for Hybrid Electric Vehicles

David G. Dorrell[1]
Senior Member

Andrew M. Knight[3]
Senior Member

Mircea Popescu[2]
Senior Member

Lyndon Evans[2]

David A. Staton[2]

[1]University of Technology Sydney
Faculty of Engineering and IT
Broadway, Sydney, NSW 2007
Australia
e-mail david.dorrell@uts.edu.au

[2]Motor Design Ltd
Ellesmere, Shropshire, SY12 0EG, UK
e-mail mircea.popescu@motor-design.com
l.evans@glyndwr.ac.uk
dave.staton@motor-design.com

[3]University of Alberta
Edmonton, AB, T6G 2V4
Canada
e-mail knight@ece.ualberta.ca

***Abstract* -- this paper describes an investigation into different motor designs for an application dictated by the performance of an existing hybrid electric vehicle drive (an internal permanent magnet motor). An induction motor and switched reluctance motor are studied. Torque over a wide speed range is required (base speed of 1500 rpm and maximum speed of 6000 rpm) and the total torque per volume is used as a key marker indicator. The efficiency is studied and efficiency plots are introduced. The issue with the design is the thermal temperature rise which affect the machines are described in the paper. At 1500 rpm very high current density exists in all the machines. At 6000 rpm the iron loss dominates. The paper illustrates that the permanent magnet motor is not the sole solution to specifying a drive motor for this application.**

***Index Terms*—permanent magnet motor, induction motor, switched reluctance motor, hybrid electric vehicles.**

I. INTRODUCTION

Recently there has been much interest in the development of hybrid electric vehicles (HEVs) and electric vehicles (EVs). Indeed, HEVs have been in production for several years and now reached a level of maturity [1]. There are also several electric vehicles and these even reach into the sports car market with high performance possible using battery-powered induction motor drives [2]. Both of these two examples use different types of drive motor.

This paper reports on a study to compare the performance of an interior permanent magnet drive motor (IPM), a copper cage induction machine (IM) and a switched reluctance machine (SRM). The design data for the IPM is taken from a report on the 2004 Toyota Prius hybrid electric vehicle drive [1] and the comparison IM uses the same stator design layout (but with an increased air-gap diameter). There is common perception that the permanent magnet motor is the correct solution for the application and offers considerable advantages in terms of performance and efficiency. However, there is little information that has been published comparing side-by side performance of equivalent designs. This is despite the fact that IM have been used to drive a number of vehicles, including the GM EV1 and the Tesla sports car [2]. Given that the future world-supply of rare-earth magnet material may be restricted [3] then it is worth considering optional arrangements and the induction motor and switched reluctance motor do have advantages over its permanent-magnet counterpart in terms of material and manufacturing costs and durability. When it is required to free-wheel it will offer energy saving in terms of removal of excitation and hence iron loss. The switched reluctance machine is already being addressed as a possible magnet-free alternative as suggested in [4] and this too offers controllable flux and zero-field coasting. Hence, both the induction motor and switched reluctance motor offer the advantage of more flexibility of flux control which, even if they cannot offer the same absolute efficiency at maximum torque at the extremities of the speed range, they may be more efficient when considering a full duty cycle, with reduced iron losses at light loading or free-wheeling.

The paper briefly describes some basic machine considerations. A *SPEED* model [5] using PC-BDC and PC-FEA for the existing 2004 Toyota Prius drive motor is developed and validated using the performance data in [1]. This takes the form or an 8 pole machine with a speed range up to 1500 rpm for base speed (maximum torque) and a maximum power range from 1500 to 6000 rpm (often called the field weakening or phase advance range). An initial induction motor design is generated using *SPEED* PC-IMD for direct simulation comparison. 2-D FEA (both static and time-stepped) models for the IM are also developed to predict torque, loss and efficiency to a more accurate detail. Options to improve the initial design, together with thermal analysis, are also presented. The same torque/speed profile is used in order to formulate the design for direct comparison. An 8-pole arrangement is again used. The frequency of the flux for these two machines is 100 Hz at 1500 rpm and 400 Hz at 6000 rpm. There is a fine balance between the copper and iron losses for this application – it is very demanding.

The IPM study and induction motor design were first

studied in [6] (which reviewed the torque/speed envelope and the reluctance/excitation torque properties and phase advance of the IPM, together with a first-pass analysis of the IM) and [7] (which addressed further analysis techniques that can be applied to the Prius IPM drive motor such as I-Psi diagrams, efficiency charts and iron loss distributions of the IPM machine). The findings from [6] and [7] are underpinned by the work in [8] and [9]. In [8] a novel wound-field machine was studied as an alternative machine the Prius drive motor. This was termed a hybrid excitation motor (HEM) which had both radial and axial flux paths as well as SMC and laminated steel core materials. It showed good promise. Switched reluctance machines (SRMs) were investigated in [9], again as an alternative to the Prius motor. In terms of stator/rotor pole numbers, 6/4, 8/6, 12/8 and 18/12 arrangements were investigated. The latter arrangement is also investigated here.

This paper will review some of the findings from [6] and [7], and add further analysis related to the induction motor analysis. In addition, a third motor option studied is the switched reluctance machine. In [4] an 18 stator pole and 12 rotor pole arrangement is suggested and this arrangement is studied in this paper. This gives 300 Hz unipolar flux at 1500 rpm and 1200 Hz at 6000 rpm so iron loss has to be carefully considered.

II. Brief Comparison of Motor Design Topologies

This paper will outline some basic analysis techniques such as the use of efficiency plots, frozen permeability method, time-stepped FEA, etc. However, to aid early comparison for clarity, it is worth putting a forward the geometrical comparison of the machines under study in this section. The three machines studied are:

- 8 pole IPM motor used in the 2004 Prius [1]
- 8 pole IM design as studied in [6] and [7]
- 18 stator pole (3-phase) 12 rotor pole SRM arrangement as suggested in [4] (but a different design as studied in [9])

The specific target application is the 2004 Prius machine as discussed in [1] and [10]. At maximum torque the current density in the windings is very high and an operating temperature of 100 ºC is assumed for the winding temperature in the results put forward here. Even though these machines have water and oil cooling it is important to consider the thermal performance of the machines. Cross sections of the three different machines are shown in Fig. 1. As previously mentioned, the IPM and IM are both 8 pole machines while the SRM has 18 stator poles and 12 rotor poles. They all share the same axial length (84 mm), inner rotor diameter (111 mm) and outer stator diameter (269 mm) in order to make direct comparison. The rotor outer diameter for the IPM is 160.5 mm; for the SRM it is 160.5 mm while for the induction motor it is 180 mm. The increases are required to meet the specification. A full description of the design procedures for the IM and SRM motors are put forward below.

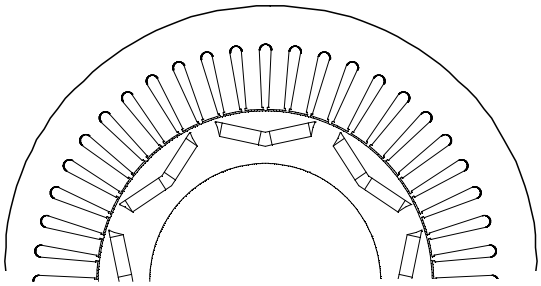

(a) Prius PM motor

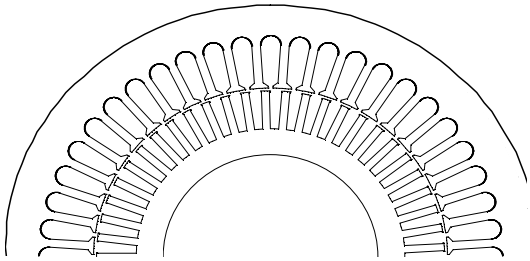

(b) Induction motor

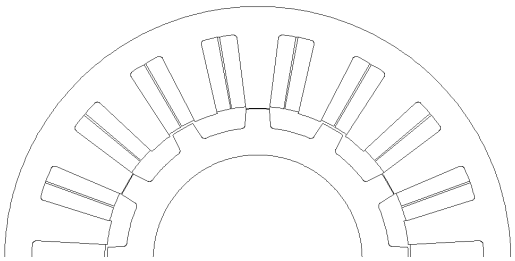

(c) Switched reluctance motor

Fig. 1. Half cross sections of the alternative motor designs.

III. Detailed Motor Analysis

A. *Review of Prius PM Drive*

A specification was given in [1] for this machine however further detailing was required to assess the design. Some of the analysis results are given in Fig. 2 for this machine. At 1500 rpm the losses are dominated by the copper loss whereas at 6000 rpm the iron loss dominates. In Fig. 1 the cross section illustrates that the machine has a high degree of q-axis saliency. This requires investigation as illustrated in Fig. 3 (a) and (b). The torque components were separated out using the "frozen permeabilities" technique [11] in the finite element analysis. The torque can be cross-checked using current – flux-linkage diagrams [12], these have been done to validate the torque and will be illustrated in the full paper. The best operation was obtained at about 60º phase advance. Finite element analysis was used to assess the iron loss using a modified Steinmetz equation [13]. The finite element bolt-

on PC-FEA was used to obtain the flux distributions for inspection and these are shown at full load at 1500 rpm (190.9 A rms) in Fig. 4 and at 6000 rpm (35.4 A rms) in Fig. 5. Even though the flux density is lower at 6000 rpm (because the current is less) the iron loss is higher because of the increase in frequency. Most of the iron loss is in the stator teeth as illustrated in Fig. 6.

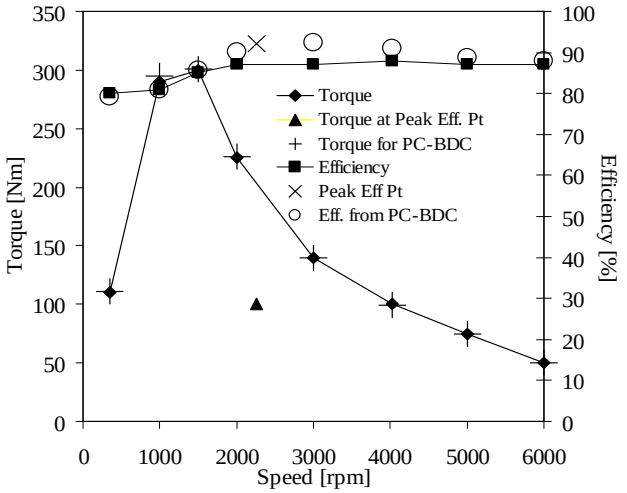

Fig. 2. Comparison of PC-BDC operating envelope with those published in [1] showing good agreement. Control maintains current on q-axis. This PC-BDC is adjusted to give the correct torque and thus the efficiency is obtained.

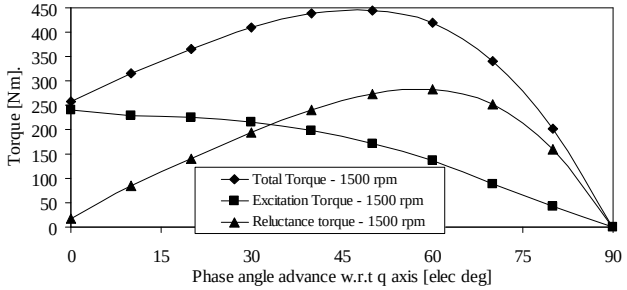

(a) Separation of torque at 1500 rpm with 190.9 A loading – variation of current phase with respect to q axis.

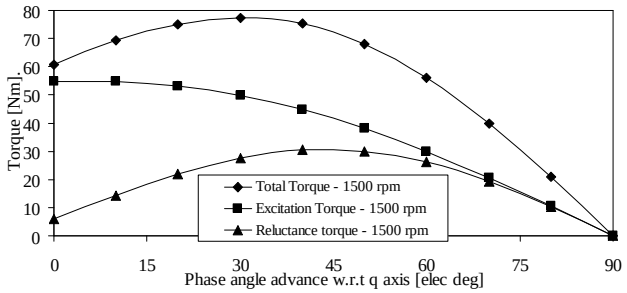

(b) Separation of torque at 6000 rpm with 35.4 A loading – variation of current phase with respect to q axis.

Fig. 3. Separation of excitation and reluctance torques at 1500 and 6000 rpm.

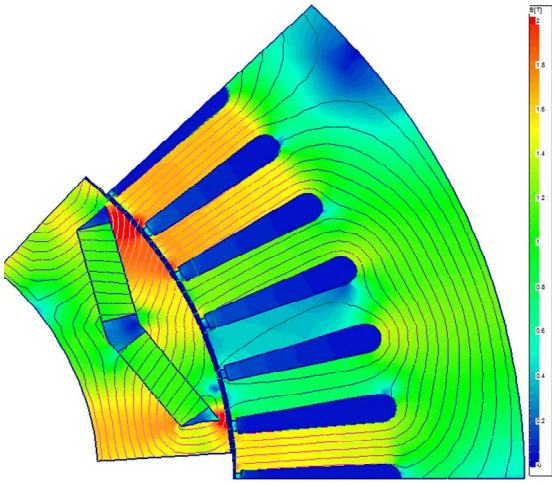

Fig. 4. One pole of machine from static FEA solution. Peak flux density in teeth is about 1.65 T. Load current 35.4 A at on the q-axis (6000 rpm).

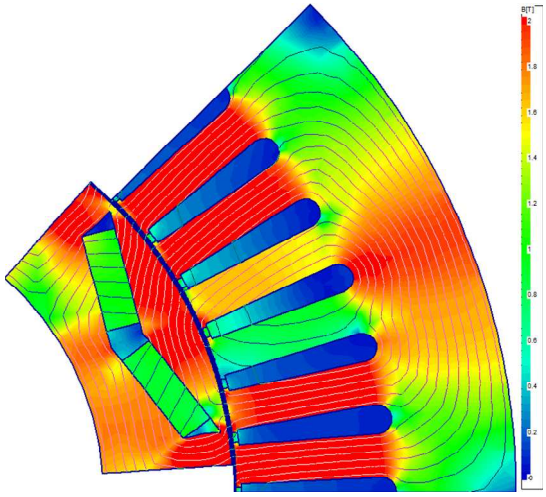

Fig. 5. One pole of machine from static FEA solution. Peak flux density in teeth is about 2.10 T. Load current 190.9 A at on the q-axis (1500 rpm).

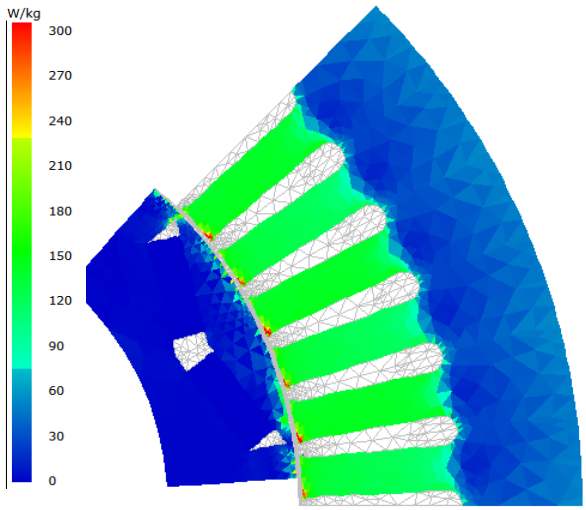

Fig. 6. Iron loss distribution from PC-FEA solution at 6000 rpm. Load current 35.4 A at on the q-axis.

An automated routine can be used to examine the efficiency of the machine over a two-dimensional torque-speed plane and a colored contour plot developed. This is shown in Fig. 7. To carry out this simulation three phase advances were used (0, 30 and 60º) and the current magnitude adjusted to obtain the required torque (Fig. 7 (a)). This efficiency plot in Fig. 7 (b) is very similar to those illustrated in [1] and similar plots will be put forward for the IM and SRM. The IM and SRM alternative designs will now be addressed and a comparison made.

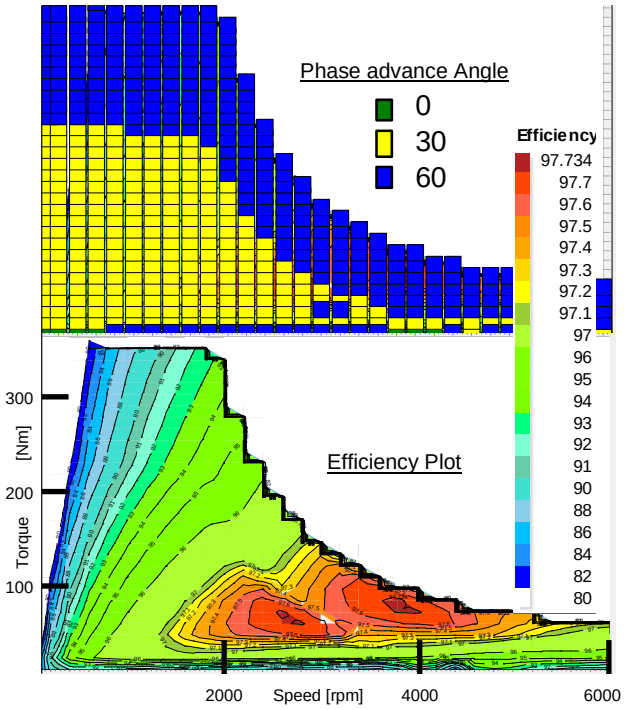

Fig. 7. Efficiency plot for PC-BDC simulations using (a) phase angles of 0, 30 and 60 degrees and (b) the efficiency predictions.

B. SRM Motor Design

The SRM design was analyzed using SPEED PC-SRD in conjunction with finite element analysis to realign the current – flux-linkage lines. The rotor radius was increased to 170 mm compared to the IPM motor but the outer stator and inner rotor radii, together with the core axial length, were maintained; the machine is a 3-phase, 18 stator pole 12 rotor pole arrangement. Here, key points at 1500 and 6000 rpm are investigated at full load. Figs. 8 to 10 show the current waveforms, current – flux-linkage loops (which are used to obtain the torque) and a flux plot when the rotor is close to alignment. This is a similar arrangement to that in [4] and [9]. In [9] a detailed study was put forward that addressed topology and materials. The paper illustrated that careful consideration of material will improved the efficiency; the authors compared 35A300 with 10JNEX900 and found the latter offered improved efficiency (between 1 and 3 %) across a full power range at 3000 rpm (for a 50 kW Prius application). In this paper M19 24 GAGE steel is used. A qualitative sizing exercise was carried out until performance was produced that matched the original IPM design.

Since this is a three phase machine and maximum pulse width is used so that there is some coupling between the phases. The stator-rotor pole combination leads to further interactions. Fig. 10 shows a finite element flux plot when an excited phase is close to alignment and the current is 300 A as shown In Fig. 8. The results shown here suggest that the SRM is capable of giving a torque per motor volume of 58 Nm/L which is slightly higher than quoted in [4] (45 Nm/L). The current density in the winding is high (20.1 Arms/mm^2) and the torque generated at the 1500 rpm peak torque point is 293 Nm with an efficiency of 85.2 %. The current – flux-linkage loops in Fig. 9 illustrate that at 1500 rpm, the loop is maximized and the machine is essentially operating close to the practically maximum torque.

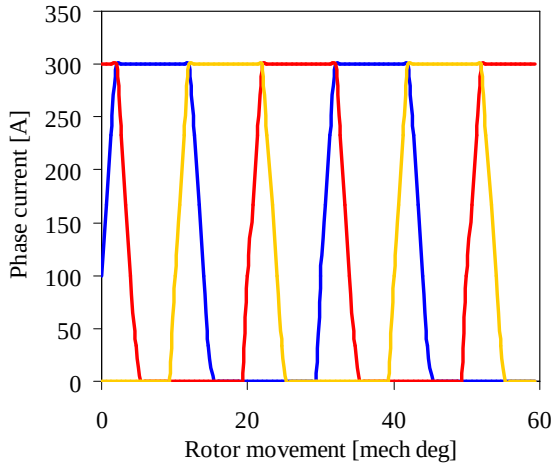

Fig. 8. Current waveforms at 1500 rpm and full load.

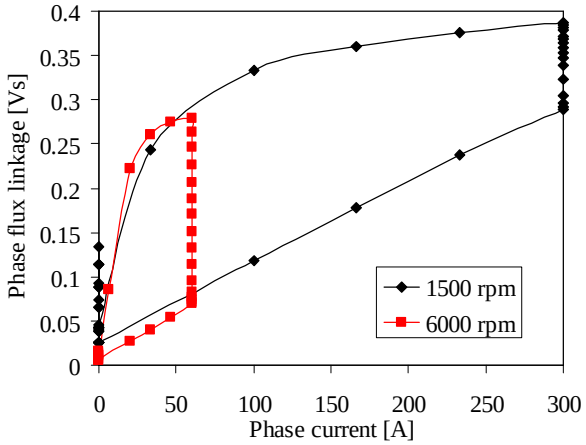

Fig. 9. I-Psi loops at at 1500 rpm (300 A peak – 293 Nm) and 6000 rpm (50 A peak – 60 Nm).

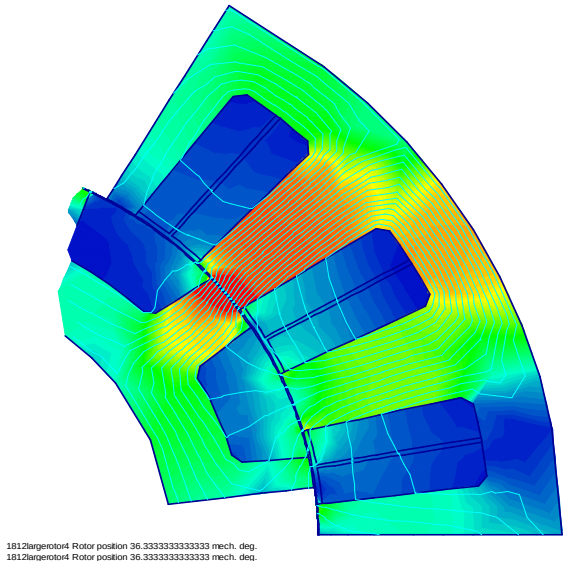

Fig. 10. Flux plot at 1500 rpm and full load current (300 A peak).

The field excitation in an SRM can be fully controlled. If the switching angles are maintained, then the torque can be controlled by variation of the peak current. This is done in Figs. 11 and 12 at the base speed and maximum speed. These show variation of torque with phase current. At 1500 rpm, where the operation at the aligned point is well past the saturation knee point, the characteristic is almost linear, whereas at 6000 rpm, it is initially non linear. This is purely a function of saturation and the shape of the I-Psi loops. The efficiency characteristics show flat characteristic for the 1500 rpm characteristic (93.4 % down to 85.1 % at peak torque) while there is more variation at 6000 rpm where is the efficiency is low (62.4 %) at low loading and increases to a peak of 88.2 % at maximum load). These are reasonable efficiencies for modern SRM design.

It can be seen that the SRM design does represent an alternative to the IPM machine described. Indeed, Fig. 3 illustrates that the IPM has a lot of q-axis saliency and the reluctance torque is higher than the excitation torque with 60 deg phase advance.

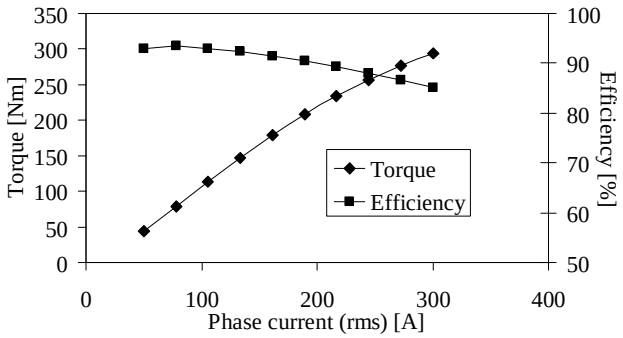

Fig. 11. Variation of current at 1500 rpm showing torque and efficiency.

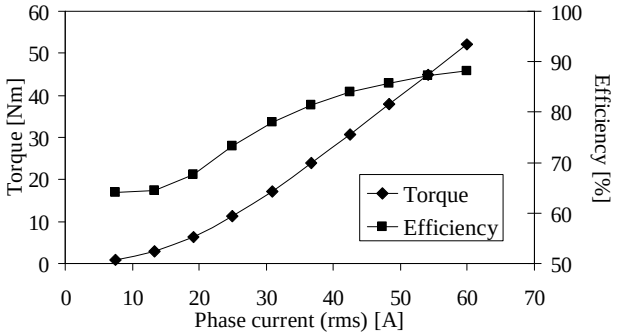

Fig. 12. Variation of current at 6000 rpm showing torque and efficiency.

C. Induction Motor Design

An induction motor design is now addressed. The IM was developed in SPEED PC-IMD to enable rapid design and tested using the static FEA bolt-on PC-FEA. To further validate the design then it was checked using time-stepped FEA.The general dimensions for the PM motor were taken and the rotor replaced with a cage rotor. Because the flux levels can be adjusted then it is possible to adjust the tooth width in the stator and the yoke thickness so. In addition, the rotor diameter can be increased in order to improve the torque-arm length and also allow deeper rotor slots; therefore the rotor diameter was now set to 180 mm. The design maintains the 8-pole 48 stator slot arrangement for this first-pass design. The bar number is 53, but for the time-stepped FEA analysis it was reduced to 40 bars simply to afford a degree of symmetry and allow a one pole periodicity; however, the rotor copper was maintained and the end-rings increased in order to obtain the same approximate performance. As already stated, a PC-IMD model was developed for this machine and passed through to PC-FEA and a flux plot for the 53 bar machine is illustrated in Fig. 13. The windings in the induction motor are rearranged in terms of series/parallel connection although the wire gauge and slot fill are maintained. More detailed description of the analysis was put forward in [7].

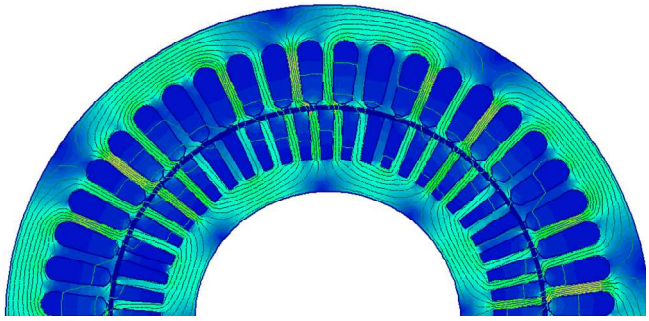

Fig. 13. Static finite element solution for 53 bar induction motor at 5960 rpm load point.

The performance of the machine was tested using a time-stepped FEA analysis at the two key points at 1500 and 6000

rpm. The bar number in the SPEED model was reduced to 40 bars to enable one-pole periodicity in the FEA and rapid solution. However, the bars and end rinds were increased to allow for similar rotor resistances. The SPEED model used M19 24 GAGE steel again – the FEA used a similar material. The results for the comparison are given in Table I. There are marked differences at 1500 rpm and this will be related to the differences in steel material and thermal effects, and also the FEA and PC-IMD analytical simulations of core saturation. In addition, with large bars, there may be additional bars losses due to eddy currents, as illustrated in Fig. 14. With further refinement of the comparison it would be expected that the results would converge. However, the aim of this paper is to illustrate the comparable effectiveness of different motors for an HEV application so the first-pass results from SPEED PC-IMD were deemed acceptable.

TABLE I
TIME-STEPPED FEA PREDICTIONS OF PERFORMANCE FOR A SKEWED ROTOR WITH 40 ROTOR BARS AND 48 STATOR SLOTS

Actual/synchronous speeds [rpm]	1475/ 1548		5960/6000	
Simulation method	Time-step FEA	PC-IMD	Time-step FEA	PC-IMD
Torque [Nm]	300	297	44.2	49.9
Line current (rms) [A]	238.4	169.9	44.5	44.6
Line voltage (rms) [V]	350	375	600	600
Power Factor	0.45	0.51	0.68	0.70
Stator Cu loss [W]	13174	7107	453	490
Rotor Cu loss [W]	3778	2303	393	212
Fe loss [W]	418	161	506	443
Efficiency [%]	71.3	81.9	88.5	95

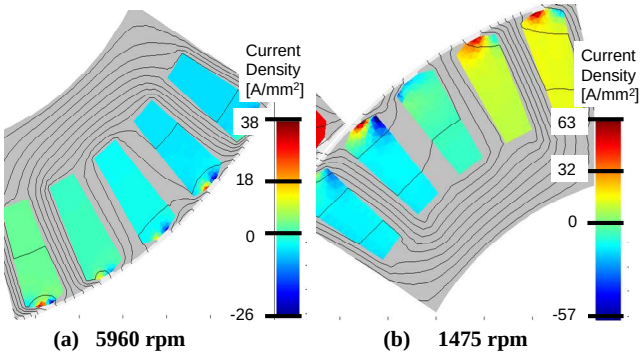

Fig. 14. Rotor bar current density showing eddy currents at slot tops.

A thermal analysis was carried out, including the fluid cooling. The analysis package (Motor-CAD) was described in [14]. The results for a basic analysis results are shown in Fig. 15. This was for the 40 bar machine. The simulation assumes coolant fluid cooling around the stator (at 20 L/min) and also down the air-gap (10 L/min). Fig. 15 shows the temperature rise for the induction machine studied in the time-stepping simulation at full load and 1500 rpm (using the loss data as calculated in Table I). It illustrates the temperature rise in key motor locations. The ambient is high and the temperature rise is shown to be 120 ºC at the centre of the stator winding. This temperature rise is similar to those reported in [10]. The induction motor is very susceptible to thermal variation as shown in [14].

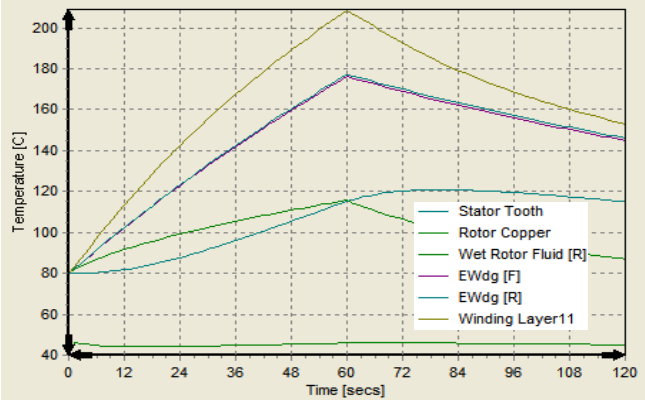

Fig. 15. Temperature rise simulation – 2 minutes at full load and 1500.

To effectively use an induction motor in this drive application then the efficiency has to be addressed. This will be a function of the voltage (which dictates the flux levels), slip (i.e., actual speed to synchronous frequency relationship) and temperature. Direct torque or flux vector control needs to be used to realize this point. This is not investigated here due space constraints but an algorithm can be developed to search for the maximum efficiency operating point at certain speed and torque demand. This requires a search for the correct voltage and synchronous frequency at a set speed, torque and temperature and this will be the focus of further work. This can also be extended to include temperature variation and study of the duty cycle. For the set point here of 1475 rpm and a frequency of 103.2 Hz (1548 rpm synchronous speed) then 350 V (line) gives the torque- and slip-speed curves and it can be shown that 1475 rpm is very close to the peak efficiency as illustrated in Fig. 16. The operating point should be close to the peak efficiency point however a full investigation needs to be carried out to study this issue.

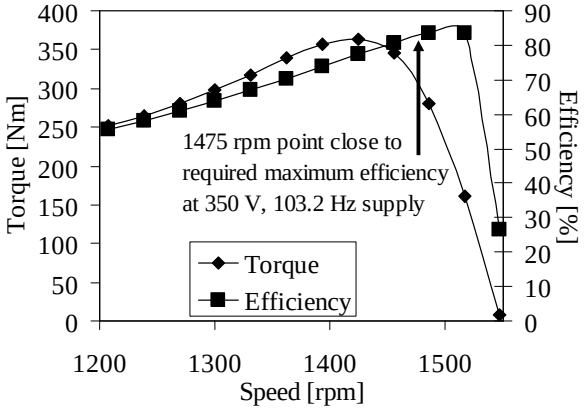

Fig. 16. Illustration of torque- and efficiency-speed curves at base speed for induction motor.

D. Comparison of Machines

In this section the three machines are studied in terms of their arrangement and operating points. Table II shows the machine geometrical parameters for the different designs put forward in this paper. It should be remembered that the IPM machine is a commercial design that will be the product of a more detailed design process than the SRM and IM designs which are first-pass electromagnetic designs aimed at investigating alternative drive technology. They illustrate that the induction motor and switched reluctance motor are alternatives to the IPM drive currently used. This paper has not addressed the power electronic drive requirements although all are 3-phase (with the SRM only requiring unipolar operation) and should be comparable. The main differences will be concerned with current and voltage ratings although these are similar given the similar power ratings.

TABLE II
COMPARISON OF PM AND INDUCTION MOTORS

Parameter	PM Motor	SRM	Induction Motor
Outer stator diameter [mm]	269.0	269.0	269.0
Inner rotor diameter [mm]	111.0	111.0	111.0
Outer rotor diameter [mm]	160.5	170.0	180.0
Air-gap length [mm[	0.73	0.3	1.5
Axial core length [mm]	84	84	84
Weight of stator core [Kg]	18.65	14.11	11.86
Weight of stator copper [Kg]	5.99	7.44	10.57
Weight of rotor core [Kg]	5.22	5.16	6.15
Weight of rotor magnet/copper [Kg]	1.30	---	7.67
Total weight [Kg]	31.16	26.71	36.25

TABLE III
COMPARISON OF PERFORMANCES AT 1500 AND 6000 RPM AT MAXIMUM POWER

Speed = 1500 rpm						
Variable	Torque [Nm]	Current [Arms or Apk- SRM]	Iron loss [W]	Copper loss [W]	Eff. [%]	RMS current density [A/mm^2]
IPM	303	141.1	198	4328	91.3	15.7
IM	297	164.8	148	8591	83.1	15.8/12.1
SRM	294	300	404	7653	85.2	20.1
Speed = 6000 rpm						
Variable	Torque [Nm]	Current [Arms or Apk- SRM]	Iron loss [W]	Copper loss [W]	Eff. [%]	RMS current density [A/mm^2]
IPM	45.6	31.8	953	219	96.1	3.75
IM	50.8	47.1	439	730	95.2	4.51/3.72
SRM	52.1	60	4074	306	88.2	4.02

The specification is demanding due to the wide speed range and the performance figures at 1500 and 6000 rpm with maximum power are given in Table III. It is interesting to note the change in dominant losses at base speed (copper losses) to full speed (iron losses). The SRM has higher iron losses due to the increased frequency of the flux, and at 1500 rpm the copper losses are high. These can be reduced with further design work. Here, a simple design is put forward for clarity. While the efficiencies are generally lower for the IM and SRM, more detailed design work will improve this and full duty cycling needs to be carried out since during coasting, they can be switched off with no losses whereas the IPM is always excited and absorbing iron-loss power, either electrically or mechanically.

It is also worth considering costs and manufacturing. Basic bare material costs are given in Table IV illustrating that the materials in the IPM are substantially higher than the IM, while the SRM is the cheapest in terms of raw materials. The IM has much more copper than either then IPM or the SRM while the cost of the IPM is dominated by the magnet cost. In terms of manufacturing, rare-earth magnet machines often have to be assembled with magnetized magnets, and they can cause issues in their handling. The SRM should be straight forward to manufacture but, as can be observed in Table II, the SRM has a much smaller air-gap length, in order to realize a high reluctance ratio, so that more precision is needed when assembling an machine with very low air-gap length.

TABLE IV
APPROXIMATE MATERIAL COSTS OF MOTOR EXCLUDING FRAME AND FITTINGS

		Laminated Steel	Copper	Neodymium Iron Boron	Totals [US$]
	US$/Kg	1.3[a]	6.6[b]	132[c]	
IPM	Weight	23.87	5.99	1.3	
	Cost	31.03	39.53	171.60	242.17
SRM	Weight	19.27	7.44	0	
	Cost	25.05	49.10	0	74.16
IM	Weight	18.01	18.24	0	
	Cost	23.41	120.38	0	143.80

[a]Lamination estimated to be approximately double bulk steel cost.
[b]London Metal Exchange, June 2010
[c]W. T. Benecki, The Permanent Magnet Industry Outlook, Great Western Minerals Group, June 2008

IV. CONCLUSIONS

This paper has put forward two additional machine designs as alternates to the IPM drive which is currently used. These are first-pass designs and the application is demanding due to the very wide maximum-power range. However, they illustrate performance that is close to the IPM and with further design refinement and thermal analysis they will meet the specification. The SRM is particularly susceptible to high iron loss. The IM and SRM will be more straightforward to manufacture and fabricate; their materials will be cheaper and they can be assembled demagnetized. The IPM is large and likely to require assembly with pre-magnetized magnets.

REFERENCES

[1] Mitch Olszewski, *Evaluation of the 2007 Toyota Camry Hybrid Synergy Drive System*, Oak Ridge National Laboratory, U.S. Department of Energy, USA, 2009.

[2] Martin Eberhard, "How Electric Vehicles Must Change the Way the Auto Industry Thinks", Plenary Session, IEEE ECCE conference, San Jose, Sept 24-28 2009.

[3] *China's Complete Control Of Global High-Tech Magnet Industry Raises U.S. National Security Alarms*, Manufacturing and Technology News, Vol. 16, No. 16, Sept. 30, 2009.

[4] M. Hamada, A. Chiba, *SR Motor Made Small Enough for Hybrid Cars*, Tech and Industry Analysis from Asia, Dec 17 2009, English version of article at web address: http://techon.nikkeibp.co.jp/english/NEWS_EN/20091217/178651/

[5] T.J.E. Miller, *SPEED's Electrical Motors*, *SPEED* Laboratory, University of Glasgow, 2006.

[6] D. G. Dorrell, M. Popescu, L. Evans, D. A. Staton and A. M. Knight, "Comparison of Permanent Magnet Drive Motor with a Cage Induction Motor Design for a Hybrid Electric Vehicle", The 2010 International Power Electronics Conference (IPEC-Sapporo), Sapporo (Japan), June 21-24 2010.

[7] D. G. Dorrell, M. Popescu, L. Evans, D. A. Staton and A. M. Knight, "Modern Electrical Machine Analysis and Design Techniques Applied to Hybrid Vehicle Drive Machines", IEEE International Symposium on Industrial Electronics (ISIE 2010), Bari (Italy), July 4-7 2010.

[8] T. Kosaka, T. Hirose and N. Matsui, "Brushless Synchronous Machines with Wound-Field Excitation using SMC Core Designed for HEV Drives," The 2010 International Power Electronics Conference (IPEC-Sapporo), Sapporo (Japan), June 21-24 2010.

[9] Y. Takano, M. Takeno, N. Hoshi, A. Chiba, M. Takemoto, S. Ogasawara and M. A. Rahman, "Design and analysis of a switched reluctance motor for next generation hybrid vehicle without PM materials," The 2010 International Power Electronics Conference (IPEC-Sapporo), Sapporo (Japan), June 21-24 2010.

[10] L. D. Marlino, *Report on Toyota Prius Motor Thermal Management*, Oak Ridge National Laboratory, U.S. Dept. of Energy, USA, 2005.

[11] J. A. Walker, D. G. Dorrell and C. Cossar, "Flux-linkage calculation in permanent-magnet motors using the frozen permeabilities method", *IEEE Trans. on Magnetics*, Vol. 41, No. 10, Oct. 2005, pp 3946 – 3948.

[12] D. A. Staton, R. P. Deodhar, W. L. Soong, and T. J. E. Miller, "Torque prediction using the flux-MMF diagram in AC, DC, and reluctance motors", *IEEE Trans. on Industry Appl*., Vol. 32, No. 1, Jan. 1996, pp 180–188.

[13] J. Reinert, A. Brockmeyer and R. W. A. A. De Doncker, "Calculation of losses in ferro- and ferrimagnetic materials based on the modified Steinmetz equation", *IEEE Trans. on Industry Appl*., Vol. 37, No. 1, July-Aug. 2001, pp 1055 – 1061.

[14] D. G. Dorrell, "Combined Thermal and Electromagnetic Analysis of Permanent Magnet and Induction Machines to Aid Calculation", *IEEE Trans. on Industrial Electronics*, Vol. 55, No. 10, October 2008 pp 3566-3574.